

Linear phase imaging using differential interference contrast microscopy

MATTHEW R. ARNISON*, KIERAN G. LARKIN†, COLIN J. R. SHEPPARD*,
NICHOLAS I. SMITH‡ & CAROL J. COGSWELL◇

September 7, 2003

* *Physical Optics Laboratory, School of Physics, University of Sydney, NSW, 2006, Australia*

† *Canon Information Systems Research Australia, 1 Thomas Holt Drive, North Ryde, NSW, 2113, Australia*

‡ *Dept. of Applied Physics, 2-1 Yamadaoka, Suita, Osaka, 565-0871, Japan*

◇ *Dept. of Electrical & Computer Engineering, University of Colorado, Boulder, CO, 80309-0425, USA*

Revised submission to Journal of Microscopy as a Short Communication

\$Date: 2003-09-07 17:00:14+10 \$ \$Revision: 1.10 \$

Running title: Linear phase imaging using DIC

Correspondence: Matthew R. Arnison is now at Canon Information Systems Research Australia, 1 Thomas Holt Drive, North Ryde, NSW 2113, Australia. Email: mra@cisra.canon.com.au.

Key words. differential interference contrast microscopy, Nomarski DIC, phase retrieval, phase shifting, spiral phase transform, Hilbert transform, Fourier transform, image processing.

Summary

We propose an extension to Nomarski differential interference contrast microscopy which enables isotropic linear phase imaging. The method combines phase shifting, two directions of shear, and Fourier-space integration using a modified spiral phase transform. We simulated the method using a phantom object with spatially varying amplitude and phase. Simulated results show good agreement between the final phase image and the object phase, and demonstrate resistance to imaging noise.

Introduction

Differential interference contrast (DIC) is a popular method for easily imaging optical path length changes in microscopic specimens (Pluta, 1989). This allows rapid inspection of unstained objects, such as biological tissues in transmission or surface heights in reflection.

While DIC is known as a phase imaging technique, four major problems persist: (1) standard DIC systems are qualitative in nature, with a non-linear response to optical path length gradients in the specimen; (2) the DIC output intensity is a mix of amplitude and phase gradient contrast; (3) for many applications it is useful to obtain the actual phase of the specimen, whereas DIC gives a directional phase gradient; and (4) it is desirable that any phase reconstruction method be straightforward, non-iterative and yet robust.

Solving these problems requires a method which:

- has a linear response to specimen phase gradient,
- isolates the phase gradient from the object amplitude signal,
- isotropically integrates the phase gradient to obtain the phase, and
- is robust and non-iterative.

Several approaches to meeting these goals have been proposed in recent years. Phase shifting DIC is a quantitative optical approach to isolating the phase gradient by shifting the DIC prism bias (Hariharan & Roy, 1996; Cogswell et al., 1997; Xu et al., 2001). While phase shifting DIC relies on a geometrical optics approximation of DIC imaging in order to isolate the phase, Ishiwata et al. (1996) demonstrated an alternative method for isolating the phase based on a partially coherent model. Their method approximates an integral with respect to the bias, by recording four images each with a different bias, then multiplying the image intensity by the sine of the DIC prism bias, and finally adding the images together to isolate the phase.

Shimada et al. (1990) briefly outline a method which at first glance solves the main three problems of linearity, phase isolation and isotropic integration. They demonstrated phase retrieval from a series of DIC images with changing prism bias and shear direction. However, the details are not clearly specified for their phase shifting and phase integration steps. In addition, their method is designed for reflection DIC, and implicitly assumes a constant object amplitude.

Approaches involving iterative computation which also only partially solve the first three problems include line integration and deconvolution (Kam, 1998), variance filtering and directional integration using iterative energy minimisation (Feineigle et al., 1996), and rotational diversity (Preza, 2000). The latter technique involves taking several rotated DIC images and combining them using iterative deconvolution. Non-iterative yet anisotropic methods include direct deconvolution (van Munster et al., 1997) and the half-plane Hilbert transform (Arnison et al., 2000) which is a qualitative Fourier-space approach to integrating the phase gradient.

To date no author has outlined a full method which completely addresses all four problems outlined above. In this communication we detail a combined optical and computational extension of DIC which solves these major problems, resulting in a phase image which is linearly proportional to the object phase and which has a laterally isotropic response to specimen phase.

Method

Our method combines four techniques. The first technique is conventional DIC microscopy. For a complex specimen amplitude of the form $a(x,y) \exp[i\phi(x,y)]$, the 2D DIC image intensity is given by

$$f_{2\theta}(x,y) = a_{1x}^2 + a_{2x}^2 + 2a_{1x}a_{2x} \cos[\phi_{1x} - \phi_{2x} + 2\theta], \quad (1)$$

where $a_{1x}(x + \Delta x, y)$ and $a_{2x}(x - \Delta x, y)$ are the amplitudes for two positions in the object separated by a shear $2\Delta x$ set by the DIC Wollaston prism, $\Delta\phi_x = \phi_{1x} - \phi_{2x}$ is the corresponding phase difference between those two positions, and 2θ is the optical DIC bias (Pluta, 1989; Cogswell & Sheppard, 1992). Here we assume geometrical optics and the Born approximation, but we do not assume a constant object amplitude. A schematic of a DIC microscope is shown in Fig. 1.

The second technique is phase shifting DIC (Hariharan & Roy, 1996; Cogswell et al., 1997; Xu et al., 2001). This technique retrieves a linear phase gradient through phase shifting by rotating the bias 2θ . The bias may be conveniently set by first inserting a quarter wave plate before the analyser. Rotating the analyser then rotates the bias (Hariharan, 1993). We can then obtain the phase gradient in the x direction using

$$\Delta\phi_x = \tan^{-1} \left(\frac{f_{\pi/2} - f_{3\pi/2}}{f_0 - f_\pi} \right), \quad (2)$$

where four DIC images f have been recorded at biases of $2\theta = 0, \pi/2, \pi, 3\pi/2$. We have now removed both the object amplitude and vignetting from the signal and obtained a linear phase gradient in the x direction. This step also removes many potential phase-independent system errors, such as weak spots on the camera or non-uniform illumination. But we have so far only imaged the component of the phase gradient which is parallel with the shear direction (van Munster et al., 1998).

The third technique is to repeat the previous two steps with the shear rotated to obtain $\Delta\phi_y$. The shear direction may be changed by rotating either the specimen or the DIC prisms by 90° . We note that a recently announced variant of DIC called total interference microscopy (Carl Zeiss, Germany) is designed to allow easy rotation of the shear angle. Combinations of DIC with multiple shear directions and phase shifting have been published previously (Hartman et al., 1980; Preza et al., 1998; Preza, 2000; Shimada et al., 1990). However in those papers a simpler phase shifting technique was applied which assumed a constant object amplitude.

Using the Fourier shift theorem, we can write down the Fourier transforms of our phase gradients

$$\Delta\phi_x(x,y) \iff 2i \sin(2\pi\Delta xm) \Phi_x(m,n) \quad (3)$$

$$\Delta\phi_y(x,y) \iff 2i \sin(2\pi\Delta yn) \Phi_y(m,n), \quad (4)$$

where m, n are the spatial frequency co-ordinates, $i = \sqrt{-1}$, \iff denotes a 2D Fourier transform, and capitalisation denotes a Fourier transformed function.

This sets the stage for the fourth technique: using Eqs. (3) and (4) to obtain the phase $\phi(x,y)$. We apply a Fourier-space integration approach which is direct, straightforward, and reasonably accurate for images that do not contain discontinuities, such

as biological phase images. We begin by combining the x and y phase gradients to form a complex function,

$$g(x,y) = \Delta\phi_x + i\Delta\phi_y . \quad (5)$$

We then perform a 2D Fourier transform on $g(x,y)$ and apply the Fourier shift theorem to give

$$\Phi(m,n) = \begin{cases} 0 & \text{if } [\sin(2\pi\Delta xm), \sin(2\pi\Delta yn)] = [0,0] \\ G(m,n)/H(m,n) & \text{otherwise} \end{cases} \quad (6)$$

with

$$H(m,n) = 2i[\sin(2\pi\Delta xm) + i\sin(2\pi\Delta yn)] . \quad (7)$$

An inverse Fourier transform of $\Phi(m,n)$ gives the desired phase $\phi(x,y)$. Phase unwrapping presents a similar problem which can be solved using a range of direct and iterative methods (Ghiglia & Pritt, 1998; Volkov et al., 2002).

For small shear distances Δx we can use $\sin x \approx x$ to approximate Eq. (7) with

$$H_d(m,n) = 4\pi i\Delta x(m + in) . \quad (8)$$

This is equivalent to approximating the phase gradients $\Delta\phi_x$ and $\Delta\phi_y$ with the partial derivatives $\partial\phi_x/\partial x$ and $\partial\phi_y/\partial y$, and then applying the Fourier derivative theorem.

Summarising the algorithm steps we have:

1. DIC imaging giving f ,
2. phase shifting giving $\Delta\phi_x$,
3. shear rotation giving $\Delta\phi_y$, and
4. Fourier phase integration giving the desired phase ϕ .

Results

We have carried out simulations to evaluate the full method. We used a coherent paraxial imaging model, which has been shown to give reasonably accurate predictions for DIC (Preza et al., 1999). However, extending our model for this simulation to include partial coherence and vectorial diffraction should not pose any fundamental difficulties.

The phantom object we simulated is shown in Fig. 2(a-b), with a transmission amplitude varying from 80% to 100% and a phase varying from 0 waves to 0.3 waves. The illuminating beam was monochromatic with wavelength $\lambda = 550$ nm, imaging the sample through a 0.5 NA lens. The shear of the DIC Wollaston prism was set at $2\Delta x = 2\Delta y = 1 \mu\text{m}$.

DIC imaging was modelled using fast Fourier transforms (FFT) with 1024×1024 pixels including windowing and padding, with the subsequent image being 363×363 pixels corresponding to a $25 \mu\text{m}$ square region of the object. DIC was simulated using the pupil functions

$$P_x(m,n) = -2i \sin(\theta + k\Delta xm) \quad (9)$$

$$P_y(m,n) = -2i \sin(\theta + k\Delta yn) , \quad (10)$$

for shear in the x and y directions respectively, where $k = 2\pi/\lambda$. We added random noise to the intensity of each simulated DIC image, generated using a uniform distribution scaled to fit between 0 and 10% of the intensity range of the image. An example simulated image is shown in Fig. 2(c). Note the image contains a mixture of amplitude and phase information, with the amplitude information geometrically distorted due to the asymmetrical pupil function in Eq. (9). We used this DIC imaging model to simulate and compute steps 2 and 3 of the algorithm. The phase gradient in the x direction $\Delta\phi_x$ is shown in Fig. 2(d).

The final step, Eqs. (6) and (7), was carried out using 726×726 pixel FFTs, after mirror reflecting the phase gradient image to significantly reduce edge discontinuity effects, as described by Ghiglia & Pritt (1998, pp. 191-192). The mirror reflection was implemented by creating a larger image g_r with four reflected copies of $g(x,y)$ inside it

$$g_r = \begin{bmatrix} g(x,y) & g(-x,y) \\ g(x,-y) & g(-x,-y) \end{bmatrix}, \quad (11)$$

before applying a Fourier transform to get $G(m,n)$. We also windowed $H(m,n)$ to avoid amplifying high frequency noise in the image, by setting $H(m,n) = 0$ for spatial frequencies outside the aperture of the simulated imaging system. Steps 1-3 took 54 s to execute on an AMD Athlon 1.4 GHz PC, while performing step 4 took 4 s.

The final phase image ϕ is shown in Fig. 2(e). This image shows we have extracted only the phase from the phantom object, with no visible corruption by either the object amplitude or random noise. After normalising both the object phase and the retrieved phase, a normalised image of the error (Fig. 2(f)) and a line plot (Fig. 3) show good agreement between the phase image and the phase of the object, with a maximum error of 16% at the edge of the image. The mean squared error is 1.5×10^{-3} .

Discussion

The retrieved phase image is qualitatively excellent. However, certain errors persist, mostly at the top and bottom edges of the image. The error in those regions is caused by the intersection of the object with the image boundary. These Fourier edge artefacts might be avoided when acquiring images experimentally by placing the spatially varying parts of the object entirely within the field of view. However, avoiding such object clipping is not always possible, which is why we have deliberately placed parts of our simulated object across the image boundary. The edge artefacts could also be removed during processing by using an improved phase integration technique at the cost of increased complexity and computation (Ghiglia & Pritt, 1998).

The results demonstrate that our method has considerable resistance to imaging noise. The retrieved phase image has no streaking artefacts, in contrast with the real-space line integration techniques described by Kam (1998) and Shimada et al. (1990). By windowing $H(m,n)$ at the same spatial frequency cutoff as that imposed by diffraction imaging, we quenched any high frequency artefacts introduced by simulated signal noise and the phase retrieval algorithm.

For simplicity in explaining our algorithm, Eqs. (1) and (2) assume geometrical optics. However, our imaging simulation included diffraction, which will attenuate

high spatial frequencies in the phase gradient and thereby introduce additional error in the retrieved phase. Yet despite our simulated object phase having a broad spatial frequency spectrum, the Fourier edge artefacts noted above produced larger errors than the geometrical optics basis of our algorithm. Supplementing our method with a deconvolution method which accounts for the effects of diffraction would produce more accurate results, effectively adding the ability to deal with spatially varying amplitudes to the approach by Preza (2000). Such deconvolution methods are generally iterative, thereby increasing the complexity and computation time relative to our non-iterative method.

Careful consideration of sampling is required to maintain high accuracy. We are assuming that the phase gradient $\Delta\phi_x$ is not too large. Unless

$$\Delta\phi_x < \pi \quad (12)$$

the DIC phase signal in Eq. (1) will wrap around. An additional limit is imposed by diffraction (Sprague & Thompson, 1972)

$$\frac{\Delta\phi_x}{2\Delta x} < k \sin \alpha . \quad (13)$$

For the system we have simulated, Eq. (12) is a tighter constraint on $\Delta\phi_x$ than Eq. (13). The size of the diffraction spot provides a tighter limit on $\Delta\phi_x$ than the shear distance only if the shear distance $2\Delta x$ is less than half the width of the brightfield point spread function (PSF), where the PSF width is defined by Sprague & Thompson (1972) to be $\lambda/\sin \alpha$. Vignetting will also affect the signal for large phase gradients.

An alternative for linear phase imaging is quantitative phase microscopy (Barty et al., 1998). This method obtains the axial intensity derivative using defocus and converts it to separate amplitude and phase images using the transport of intensity equation (TIE). One important difference to our technique is that the TIE image contrast for fine phase details decreases with higher condenser apertures (Barone-Nugent et al., 2002; Sheppard, 2002), whereas DIC imaging gives the best contrast and resolution at the largest condenser apertures.

It is interesting to note that the phase integration method in Eqs. (5-7) is related to the Hilbert transform, especially when expressed in the approximate form in Eq. (8). H_d may be rewritten as

$$H_d(m, n) = 4\pi i \Delta x \sqrt{m^2 + n^2} \exp[i \arctan(n/m)] . \quad (14)$$

Applying the spiral phase term $\exp[i \arctan(n/m)]$ in Fourier space has been proposed as a 2D version of the Hilbert transform, which is traditionally defined in 1D only (Larkin et al., 2001). It is also known as a complex Riesz transform. This 2D Hilbert transform is isotropic, as compared with the anisotropic 2D half-plane Hilbert transform outlined by Arnison et al. (2000). While both the modified spiral phase transform in Eq. (14) and the 2D Hilbert transform proposed by Larkin et al. are isotropic, our modified spiral differs by virtue of the amplitude weighting, present in Eq. (14) as the square root term.

In conclusion, we have detailed an extension of DIC which enables isotropic linear phase imaging using phase shifting, two directions of shear, and non-iterative Fourier

phase integration incorporating a modified spiral phase transform. Simulated results show good agreement between the final phase image and the object phase, for a 2D phantom object with spatially varying amplitude and phase. The method can in principle be used with any DIC imaging system, with potential applications including biological microscopy, 3D visualisation, surface profiling, refractive index profiling, and x-ray microscopy (David et al., 2002; Kaulich et al., 2002).

Acknowledgements

This work was supported by the Australian Research Council.

References

- Arnison M.R., Cogswell C.J., Smith N.I., Fekete P.W. & Larkin K.G. (2000) Using the Hilbert transform for 3D visualisation of differential interference contrast microscope images. *J. Microsc.*, **199**, 79–84.
- Barone-Nugent E., Barty A. & Nugent K. (2002) Quantitative phase-amplitude microscopy I: optical microscopy. *J. Microsc.*, **206**, 194–203.
- Barty A., Nugent K.A., Paganin D. & Roberts A. (1998) Quantitative optical phase microscopy. *Opt. Lett.*, **23**, 817–819.
- Cogswell C.J. & Sheppard C.J.R. (1992) Confocal differential interference contrast (DIC) microscopy: including a theoretical analysis of conventional and confocal DIC imaging. *J. Microsc.*, **165**, 81–101.
- Cogswell C.J., Smith N.I., Larkin K.G. & Hariharan P. (1997) Quantitative DIC microscopy using a geometric phase shifter. *Proc. SPIE*, vol. 2984, pp. 72–81. San Jose, CA, USA.
- David C., Nöhammer B., Solak H.H. & Ziegler E. (2002) Differential x-ray phase contrast imaging using a shearing interferometer. *Appl. Phys. Lett.*, **81**, 3287–3289.
- Feineigle P.A., Witkin A.P. & Stonick V.L. (1996) Processing of 3D DIC microscopy images for data visualisation. *Proc. IEEE International conference on acoustics, speech, and signal processing*, vol. 4, pp. 2160–2163. IEEE, New York.
- Ghiglia D.C. & Pritt M.D. (1998) *Two-dimensional phase unwrapping : theory, algorithms, and software*. Wiley, New York, USA.
- Hariharan P. (1993) The Sénarmont compensator: an early application of the geometric phase. *J. Mod. Opt.*, **4**, 2061–2064.
- Hariharan P. & Roy M. (1996) Achromatic phase-shifting for two-wavelength phase-stepping interferometry. *Opt. Commun.*, **126**, 220–222.

- Hartman J.S., Gordon R.L. & Lessor D.L. (1980) Quantitative surface topography determination by Nomarski reflection microscopy. II. Microscope modification, calibration, and planar sample experiments. *Appl. Opt.*, **19**, 2998–3009.
- Ishiwata H., Itoh M. & Yatagai T. (1996) Retardation modulated differential interference microscope and its application to 3-D shape measurement. *Proc. SPIE*, **2873**, 21–24.
- Kam Z. (1998) Microscopic differential interference contrast image processing by line integration (LID) and deconvolution. *Bioimaging*, **6**, 166–176.
- Kaulich B., Wilhein T., Di Fabrizio E., Romanato F., Altissimo M., Cabrini S., Fayard B. & Susini J. (2002) Differential interference contrast x-ray microscopy with twin zone plates. *J. Opt. Soc. Am. A*, **19**, 797–806.
- Larkin K.G., Bone D.J. & Oldfield M.A. (2001) Natural demodulation of two-dimensional fringe patterns. I. General background of the spiral phase quadrature transform. *J. Opt. Soc. Am. A*, **18**, 1862–1870.
- Pluta M. (1989) *Advanced Light Microscopy: Specialised Methods*, vol. 2. Elsevier, Amsterdam.
- Preza C. (2000) Rotational-diversity phase estimation from differential-interference-contrast microscopy images. *J. Opt. Soc. Am. A*, **17**, 415–424.
- Preza C., Snyder D.L. & Conchello J.A. (1999) Theoretical development and experimental evaluation of imaging models for differential-interference-contrast microscopy. *J. Opt. Soc. Am. A*, **16**, 2185–2199.
- Preza C., van Munster E.B., Aten J.A., Snyder D.L. & Rosenberger F.U. (1998) Determination of direction-independent optical path-length distribution of cells using rotational-diversity transmitted-light differential interference contrast (DIC) images. *Three-dimensional and multidimensional microscopy: image acquisition and processing V*, vol. 3261, pp. 60–70. International Society for Optical Engineering (SPIE), San Jose, California, USA.
- Sheppard C.J.R. (2002) Three-dimensional phase imaging with the intensity transport equation. *Appl. Opt.*, **41**, 5951–5955.
- Shimada W., Sato T. & Yatagai T. (1990) Optical surface microtopography using phase-shifting Nomarski microscope. *Proc. SPIE*, **1332**, 525–9.
- Sprague R.A. & Thompson B.J. (1972) Quantitative visualization of large variation phase objects. *Appl. Opt.*, **11**, 1469.
- van Munster E.B., van Vliet L.J. & Aten J.A. (1997) Reconstruction of optical path-length distributions from images obtained by a wide-field differential interference contrast microscope. *J. Microsc.*, **188**, 149–157.

- van Munster E.B., Winter E.K. & Aten J.A. (1998) Measurement-based evaluation of optical pathlength distributions reconstructed from simulated differential interference contrast images. *J. Microsc.*, **191**, 170–176.
- Volkov V.V., Zhu Y. & De Graef M. (2002) A new symmetrized solution for phase retrieval using the transport of intensity equation. *Micron*, **33**, 411–416.
- Xu Y., Xu Y.x., Hui M. & Cai X. (2001) Quantitative surface topography determination by differential interference contrast microscopy. *Opt. Precision Eng.*, **9**, 226–229.

List of Figures

1	Optical layout of a DIC microscope. In addition to the standard DIC imaging components, a quarter wave plate is shown, which enables convenient adjustment of the DIC bias.	11
2	Linear phase imaging simulation results. (a) Object transmission amplitude. (b) Object phase. (c) Simulated DIC image with shear in the x (horizontal) direction, bias $2\theta = 3\pi/2$ and artificial imaging noise at 10% of the signal. (d) Phase shifted DIC image $\Delta\phi_x$. This step isolates the phase gradient from the DIC image. (e) Final retrieved phase from our algorithm. The object amplitude, noise and directional phase shading have all been removed by our algorithm, leaving an image which is a close match to the object phase shown in (b). (f) Phase error between the normalised object phase and the normalised retrieved phase. Note the only large errors are where the phase object meets the upper and lower edges of the image. The width of the field of view is $25\mu\text{m}$. . .	12
3	A one dimensional line plot through Fig. 2, vertically downwards from the image centre. Shown are the object amplitude, object phase, DIC image with shear in the x direction and the final phase image from our algorithm. The latter three values have been normalised to enable comparison. The horizontal axis is in microns and the vertical axis is in normalised units. The retrieved phase has been effectively isolated from the object amplitude and signal noise. The error due to Fourier edge artefacts increases as the plot moves away from the centre of the image.	13

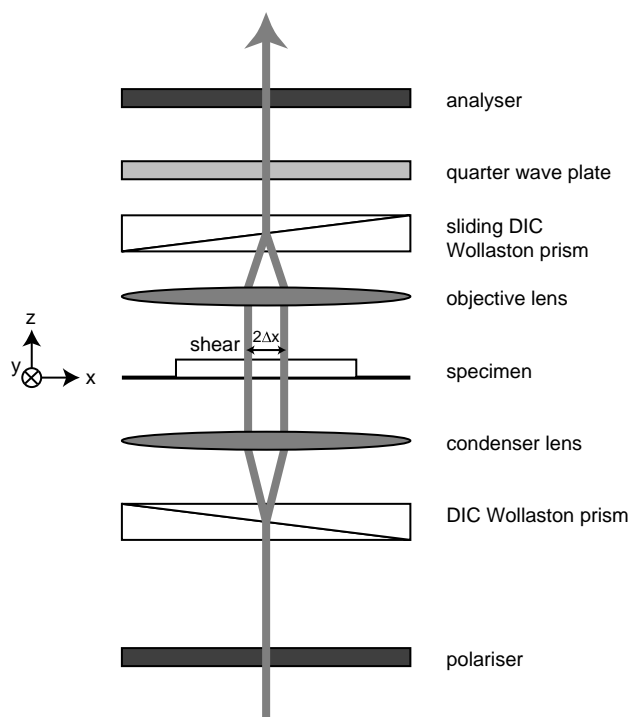


Figure 1: Optical layout of a DIC microscope. In addition to the standard DIC imaging components, a quarter wave plate is shown, which enables convenient adjustment of the DIC bias.

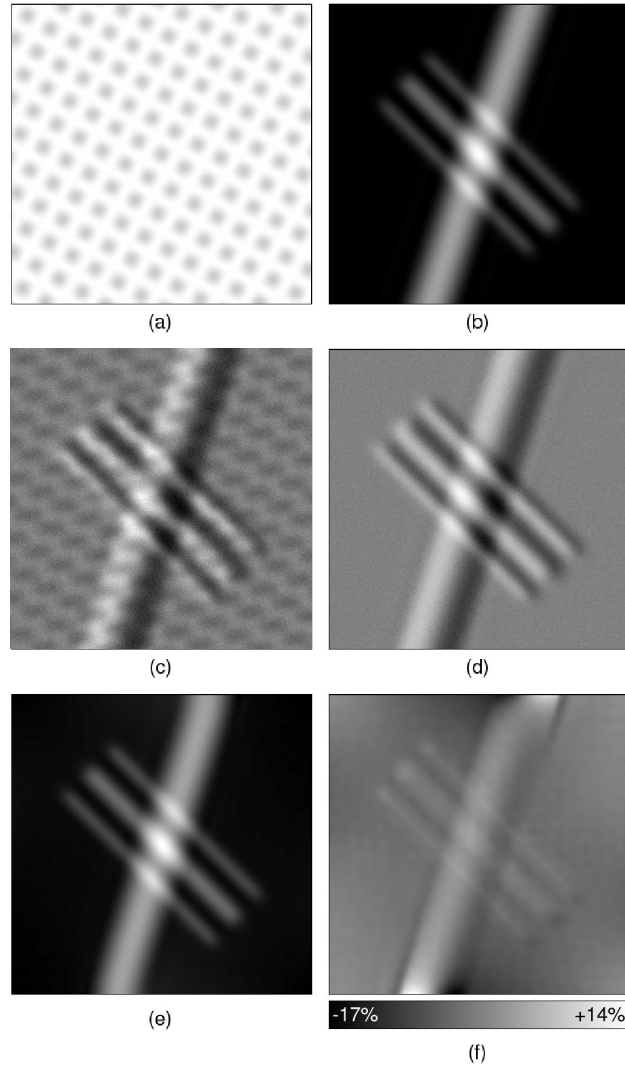


Figure 2: Linear phase imaging simulation results. (a) Object transmission amplitude. (b) Object phase. (c) Simulated DIC image with shear in the x (horizontal) direction, bias $2\theta = 3\pi/2$ and artificial imaging noise at 10% of the signal. (d) Phase shifted DIC image $\Delta\phi_x$. This step isolates the phase gradient from the DIC image. (e) Final retrieved phase from our algorithm. The object amplitude, noise and directional phase shading have all been removed by our algorithm, leaving an image which is a close match to the object phase shown in (b). (f) Phase error between the normalised object phase and the normalised retrieved phase. Note the only large errors are where the phase object meets the upper and lower edges of the image. The width of the field of view is $25\mu\text{m}$.

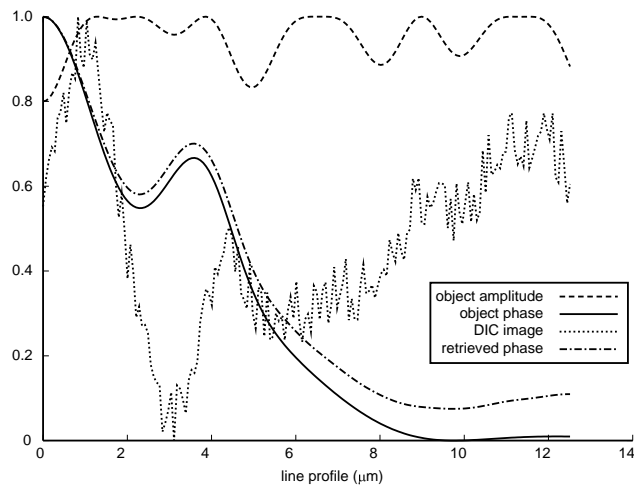


Figure 3: A one dimensional line plot through Fig. 2, vertically downwards from the image centre. Shown are the object amplitude, object phase, DIC image with shear in the x direction and the final phase image from our algorithm. The latter three values have been normalised to enable comparison. The horizontal axis is in microns and the vertical axis is in normalised units. The retrieved phase has been effectively isolated from the object amplitude and signal noise. The error due to Fourier edge artefacts increases as the plot moves away from the centre of the image.